

Comparative Study of Plasma Focus Machines

by

Arwinder Singh A/L Jigiri Singh

being a thesis submitted to
INTI International University
in candidature for the degree of
Doctor of Philosophy

Centre for Plasma Research
INTI International University
2015



INTI
International University
LAUREATE INTERNATIONAL UNIVERSITIES

**POSTGRADUATE PROGRAMME
CERTIFICATION OF DOCTORAL THESIS**

Author's Full Name : Arwinder Singh Jigiri Singh
Student I.D : 111009027
Thesis Title : Comparative Study of Plasma Focus Machines
Academic Session : May 2012 – May 2015

With regard to Clause 4.2 of the INTI Student Intellectual Property Policy (Supplementary), the thesis is the student's property. Thereby declare this thesis as:

CONFIDENTIAL

☐

Consisting of classified information under the OFFICIAL SECRETS ACT 1972.

RESTRICTED

☐

Consisting of RESTRICTED information which has been determined by the organisation/body where the research was conducted.

OPEN ACCESS/NON-RESTRICTED

☒

I allow this thesis to be published through open access, full text or copied for study, learning and research purposes only.

For the Open Access/Non-Restricted category, I allow this (Master's/Doctoral) thesis to be kept in the INTI International University (INTI) Library with the following usage conditions:

1. INTI Library has the right to reproduce the thesis for study, learning and research purposes only.
2. INTI Library is allowed to make one (1) copy of this thesis for exchange purpose among higher education institutions and any government body/agency, subject to terms and conditions.

VERIFIED BY:

ASJ

STUDENT SIGNATURE

Daw

SUPERVISOR'S
SIGNATURE

621231-07-5141

(IDENTITY CARD/PASSPORT
NO.)

Date: 11/3/2015

Professor Dr. Saw Sor Heoh
Director

SUPERVISOR'S NAME
Centre for Plasma Research
INTI International University

Date: 11/3/2015

COPYRIGHT

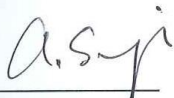
The copyright of this thesis belongs to the author under the terms of the Copyright Act 1987 as qualified by Section 4 of INTI International University Intellectual Property Policy. Due acknowledgement shall always be made of the use of any material contained in, or derived from, this thesis.

© Arwinder Singh, 2015

All rights reserved

DECLARATION

I hereby declare that the work has been done by myself and no portion of the work contained in this thesis has been submitted in support of any application for any other degree or qualification of this or any other university or institute of learning.


Arwinder Singh

ACKNOWLEDMENTS

Waheguru ji ka Khalsa, Waheguru ji ki Fateh. I firstly wish to express my deepest gratitude and thanks to both my supervisor Professor Saw Sor Heoh and my mentor Professor Lee Sing for their kind directions and inspiring guidance throughout this PhD course. Without their patience and encouragement, this thesis would never have been completed. I am very grateful to have such dedicated and encouraging supervisors.

I am also very grateful to Professor Paul Lee and Professor Rajdeep Singh Rawat of National Institute of Education, Nanyang Technological University, Singapore for their invaluable suggestions and generous help when I have difficulties.

I would also wish to express thanks to Dr Tania Davari, R A Behbahani, Professor Tanu Lass, Metrofanis Konstantin, Dr Rahindra Kumar Rout and Dr Brian Bures for providing me with the parameters and the current waveforms of the PPRC PF device, University of Tehran plasma focus, PF12, PF3, BARC plasma focus and the AASC plasma focus

Finally, I am deeply indebted to my late father, Mr. Jigiri Singh, my mother Madam Mukhtiar Kaur, my wife Pritam Kaur and my two lovely daughters Arpita Kaur Bedi and Pavandeep Kaur for all their support and understanding. I cannot find words to express my appreciation.

I acknowledge research grants INT-CPR-01-02-2012 and FRGS/2/2013/SG02/ INTI/01/1 in the research and preparation of this thesis.

ABSTRACT

The Lee Model code is a very powerful and convenient numerical experiment facility. This thesis analysed 44 Mather-type plasma focus (PF) machines operating in Deuterium, Neon and Argon; obtaining reasonably good fits for all machines so that realistic PF properties are computed and presented. Even the Speed-2 PF machine which uses a Marx bank is reasonably modelled and analysed. Also for Filippov-type PF machines, the computed current traces could be fitted to the measured only up to about half of the rising current trace.

For optimised low-inductance Type-1 machines (typically those in the region of or below 50 nH) the Lee Model 5-phase code is sufficient to fit the measured current traces. Those not properly time-matched may require the Lee Model 6-phase code to complete the fitting of the extended parts of the measured current dip. Type-2 high inductance machines (typically those above 100 nH) require the Lee Model 6-phase code even for optimised condition. The Lee Model 5-phase code is used to start the analysis of a machine, and when necessary proceeds to use the Lee Model 6-phase code to complete the fitting of any extended current dip. The code is found useful for testing whether machines are optimised or not. This has been the case of the India-Assam PF machine with electrodes designed to work in a different energy range. The code also assists in guiding the experimental process towards optimised operation as was the case for NX3. In analyzing radiation yields, it is found that the computed optimised neutron yield agrees with the measured maximum yield (difference between computed and measured being a factor about 3); the computed and available measured neon SXR yields agree in both optimised yields as well as yield versus pressure curves. Data from the machines studied was combined with that from existing machines to obtain neutron, Ne lines and Ar all-lines scaling laws.

One final observation is that, the Slow Focus Mode (SFM) is encountered at the highest pressure at which a pinch just occurs. This SFM produces a much larger pinch cross-section which may be a desirable property for deposition of advanced materials and nano-materials.

TABLE OF CONTENTS

	Page
COPYRIGHT	ii
DECLARATION	iii
ACKNOWLEDGEMENT	iv
ABSTRACT	v
TABLE OF CONTENTS	vi
LIST OF TABLES	x
LIST OF FIGURES	xxi
CHAPTER 1 INTRODUCTION	1
1.1 Background	1
1.2 Problem statement	2
1.3 Objective	2
1.4 Literature Review	3
1.4.1 Numerical Experiments	6
1.4.2 Neutron Yield	9
1.4.3 Radiation Yield	9
1.5 The Lee Model	10
1.6 Layout of the thesis	15
CHAPTER 2 METHODOLOGY	17
2.1 Introduction	17
2.2 The current fitting technique	18
2.3 Type 1 (T1) and Type 2 (T2) machine	23
2.4 Type 1 (T1) machine that shows Type 2 (T2) characteristics	24
2.5 NX2 Plasma Focus machine	24
2.6 INTI Plasma Focus machine	26

	Page
CHAPTER 3 RESULTS FROM DENSE PLASMA FOCUS MACHINES	28
BELOW 2.5 kJ FOR DEUTERIUM, ARGON AND NEON	
3.1 Introduction	28
3.2 PF50 Plasma Focus machine	30
3.3 BARC Plasma Focus 1 machine	34
3.4 AASC Plasma Focus machine	39
3.5 Argentina nanofocus machine	43
3.6 FMPF-1 Plasma Focus machine	47
3.7 India's smallest sealed type Plasma Focus machine	51
3.8 PF400 Plasma Focus machine	55
3.9 NX1 Plasma Focus machine	59
3.9.1 Case of early focus	60
3.8.2 Case of late dip	63
3.10 PPRC Plasma Focus machine	67
3.11 Kansas State University Plasma Focus machine	73
3.12 Imperial college Plasma Focus machine	78
3.13 NX2 Plasma Focus machine	81
3.13.1 Case1(C1)	82
3.13.2 Case2(C2)	85
3.13.3 Case3(C3)	86
3.13.4 NX2-T Plasma Focus machine	88
3.14 Paco Plasma Focus machine	91
3.15 University of Teheran Plasma Focus machine	96
3.16 Montecucolino Plasma Focus machine	102
3.17 DPF 2.2 Plasma Focus machine	105
CHAPTER 4 RESULTS FROM DENSE PLASMA FOCUS MACHINES	108
ABOVE 2.5 kJ FOR DEUTERIUM, ARGON AND NEON	
4.1 Introduction	108
4.2 PF12 Plasma Focus machine	109
4.3 Amir Kabir Plasma Focus machine	112

	Page
4.4	INTI Plasma Focus machine 122
4.5	Syrian Plasma Focus machine 129
4.6	Bora Plasma Focus machine 131
4.7	Hanyang University Plasma Focus machine 134
4.8	GN1 Plasma Focus machine 140
4.9	FNII Plasma Focus machine 152
4.10	Assam Plasma Focus machine 155
4.11	NX3 Plasma Focus machine 158
4.11.1	The current waveform fit at 12kV, 2.28 Torr deuterium gas 159
4.11.2	The current waveform fit at 12kV, 3.75 Torr deuterium gas 160
4.11.3	The current waveform fit at 13kV, 3.0 Torr deuterium gas 161
4.11.4	The current waveform fit at 14kV, 3.75 Torr deuterium gas 162
4.12	BARC Plasma Focus 2 machine 168
4.13	PF143 Plasma Focus machine 171
4.14	DPF78 Plasma Focus machine 177
4.15	Tamu Plasma Focus machine 182
4.16	Poseidon Plasma Focus machine 184
4.17	PF1000 Plasma Focus machine 188
CHAPTER 5	RESULTS FROM DENSE PLASMA FOCUS MACHINES 191
	USING OTHER GASES AND OTHER
	CONFIGURTIONS
5.1	Introduction 191
5.2	India Mohanty Plasma Focus machine 192
5.3	Sofia Plasma Focus machine 202
5.4	Zimbabwe Plasma Focus machine 205
5.5	Nano Focus machine (PF 0.2 Joules) 209
5.6	QUAID I AZAM University Plasma Focus machine 212
5.7	Egypt Plasma Focus machine 214
5.8	PFMA-1 Plasma Focus machine 216
5.9	Rico Plasma Focus machine 218

	Page
5.10 PF 3 Plasma Focus machine (Filippov configuration)	220
5.11 Dena Plasma Focus machine (Filippov configuration)	223
5.12 Speed 2 Plasma Focus machine	227
5.13 University Malaya Plasma Focus machine	229
CHAPTER 6 DISCUSSIONS	233
6.1 Introduction	233
6.2 Investigation	234
6.3 Machines working in deuterium gas medium	236
6.4 Machines working in neon gas medium	243
6.5 Machines working in argon gas medium	246
CHAPTER 7 CONCLUSIONS	249
7.1 Introduction	249
7.2 Observations obtained from the comparative study	249
7.3 Comparison of computed yields and measured yields	250
7.4 Scaling and Related scaling laws obtained from this study	252
7.5 Observation of Slow Focus Mode in relative high pressure machine	253
REFERENCES	254
LIST OF PUBLICATIONS	265

LIST OF TABLES

	Page
 CHAPTER 2	
2.1 The actual machine, operational and fitting parameters configured for the INTI Plasma Focus.	21
2.2 An example of the values of the anomalous resistance used to fit the INTI Plasma Focus shot for Figures 2.3 and 2.4.	22
 CHAPTER 3	
3.1 The machine, operational and fitting parameters for PF50 Plasma Focus machine.	31
3.2 Information obtained from Lee Model 5-phase code configured for PF50 Plasma Focus machine at 29kV, 6.8 Torr deuterium gas.	32
3.3 The machine, operational and fitting parameters for INDIA- BARC Plasma Focus 1 machine.	34
3.4 Information obtained from Lee Model 6-phase code configured for INDIA-BARC Plasma Focus 1 machine at 4.2 kV, 1.2 Torr hydrogen gas.	35
3.5 The operational and fitting parameters for INDIA- BARC Plasma Focus 1 machine working in deuterium gas.	36
3.6 Information obtained from Lee Model 6-phase code configured for INDIA- BARC Plasma Focus 1 machine at 4.3 kV, 1.2 Torr deuterium gas.	37
3.7 The machine, operation and fitting parameters for AASC Plasma Focus machine.	40
3.8 Information obtained from Lee Model 6-phase code configured for AASC Plasma Focus machine at 4kV, 2.9 Torr deuterium gas.	41
3.9 Machines, operational and fitting parameters for Argentina Nano Focus machine.	44

		Page
3.10	Information obtained from Lee Model 5-phase code configured for Argentina Nano Focus Machine at 16kV, 1.5 Torr deuterium gas.	45
3.11	The machine, operational and fitting parameters for FMPF-1 Plasma Focus machine.	48
3.12	Information obtained from Lee Model 5-phase code configured for FMPF-1 Plasma Focus machine at 12kV, 2.25 Torr deuterium gas.	49
3.13	The machine, operation and fitting parameters for India's smallest seal- type Plasma Focus machine	52
3.14	Information obtained from Lee Model 6-phase code configured for India's smallest sealed-type Plasma Focus machine at 10 kV, 6.0 Torr deuterium gas	54
3.15	The machine, operation and fitting parameters for PF400 Plasma Focus machine.	56
3.16	Information obtained from Lee Model 5-phase code configured for PF400 Plasma Focus machine at 28kV, 6.6 Torr deuterium gas.	57
3.17	Machines bank and focus tube parameters for NX1 Plasma Focus machine operating in Neon	59
3.18	The machine, operation and fitting parameters for NX1 Plasma Focus machine when focus came early.	60
3.19	Information obtained from Lee Model 6-phase code configured for NX1 Plasma Focus machine at 10kV, 3.0 Torr neon gas.	62
3.20	Machine and model parameters for NX1 Plasma Focus machine when dip comes late.	63
3.21	Information obtained from Lee Model 5-phase code configured for NX1 Plasma Focus machine at 14kV, 11.0 Torr neon gas.	64

		Page
3.22	The machine and operation parameters for PPRC Plasma Focus machine operating in Argon.	67
3.23	Current and mass factors as well as anomalous resistance values of PPRC Plasma Focus machine working at 14.2kV, 0.3 Torr argon gas.	68
3.24	Current and mass factors as well as anomalous resistance values of PPRC Plasma Focus machine working at 18.5kV, 0.15 Torr argon gas.	69
3.25	Current and mass factors as well as anomalous resistance values of PPRC Plasma Focus machine working at 19kV, 0.7 Torr argon gas.	70
3.26	Current and mass factors as well as anomalous resistance values of PPRC Plasma Focus machine working at 18kV, 0.3 Torr argon gas.	71
3.27	Comparison on information about PPRC Plasma Focus machine working at different pressure and charged voltage obtained from Lee Model 6-phase code when computed current waveform is compared to the measured current waveform.	72
3.28	Machines operational and fitting parameters for KSU-PF2 Plasma Focus machine.	73
3.29	Information obtained from Lee Model 6-phase code configured for KSU-PF2 Plasma Focus machine at 17 kV, 3.0 Torr deuterium gas	74
3.30	Machines operational and fitting parameters for KSU-PF2 Plasma Focus machine with 125 nH inductance at 1.125 Torr neon gas.	76
3.31	Information obtained from Lee Model 6-phase code configured for KSU-PF2 Plasma Focus machine at 17 kV, 1.125 Torr neon gas.	77

		Page
3.32	The machine, operational and fitting parameters for Imperial College Plasma Focus machine.	78
3.33	Information obtained from Lee Model 5-phase code configured for Imperial College Plasma Focus machine at 38kV, 2.62 Torr deuterium gas.	79
3.34	The machine, operational and fitting parameters for NX2 Plasma Focus machine with 3 different anode lengths, charging voltages, operating pressures and model parameters	81
3.35	Information obtained from Lee Model 5-phase code configured for NX2 Plasma Focus machine.	82
3.36	The machine, operation and fitting parameters for NX2-T Plasma Focus machine	89
3.37	Information obtained from Lee Model 5-phase code configured for NX2-T Plasma Focus machine at 12.5kV, 10.6 Torr deuterium gas.	90
3.38	The machine, operation and fitting parameters for Paco Plasma Focus machine.	92
3.39	Information obtained from Lee Model 5-phase code configured for Paco Plasma Focus machine at 31kV, 1.35 Torr deuterium gas.	93
3.40	The machine and operational parameters for University of Tehran Plasma Focus machine.	96
3.41	Fitted current and mass factors of University of Tehran Plasma Focus machine working at 0.375 Torr argon (st1, st2 and st3).	96
3.42	Fitted anomalous resistance parameters of University of Tehran Plasma Focus machine working at 0.375 Torr argon (st1, st2 and st3).	97
3.43	Comparison of computed plasma parameters for 3 different shots fired at 19kV, 0.375 Torr argon gas in University of Tehran Plasma Focus machine.	100

		Page
3.44	The machine, operational and fitting parameters for Montecucolino Plasma Focus machine.	102
3.45	Information obtained from Lee Model 5-phase code configured for Montecucolino Plasma Focus machine at 25kV, 2.0 Torr deuterium gas.	103
3.46	The machine, operational and fitting parameters for DPF2.2 Plasma Focus machine.	106
3.47	Information obtained from Lee Model 6-phase code configured for DPF2.2 Plasma Focus machine at 18kV, 11.0 Torr deuterium gas.	107
CHAPTER 4		
4.1	The machine, operational and fitting parameters for PF12 Plasma Focus machine.	110
4.2	Information obtained from Lee Model 5-phase code configured for PF12 Plasma Focus Machine at 16kV, 3.5 Torr deuterium gas.	111
4.3	The machine, operational and fitting parameters for Amirkabir Plasma Focus machine working in argon gas.	113
4.4	Information obtained from Lee Model 6-phase code configured for Amirkabir Plasma Focus machine at 12 kV, 1.26 Torr argon gas.	114
4.5	Information from Figure 4.6 presented in a table format.	116
4.6	The operational and fitting parameters for Amirkabir Plasma Focus machine working in neon gas.	118
4.7	Information obtained from Lee Model 6-phase code configured for Amirkabir Plasma Focus machine at 12 kV, 4.5 Torr neon gas.	119
4.8	Information from Figure 4.10 presented in a table format.	121
4.9	The operational and fitting parameters for UNU/ICTP PFF Plasma Focus machine.	122

		Page
4.10	The anomalous resistances Dip value for UNU/ICTP PFF machine when working in argon gas medium (13.5kV, 1.5 Torr), deuterium gas medium (13.5 kV, 3.0 Torr) and neon gas (12kV, 2.0 Torr and 14kV, 2.8 Torr) respectively.	125
4.11	Information obtained from Lee Model 6-phase code configured for UNU-ICTP Plasma Focus machine working in neon gas (12kV, 2.0 Torr and 14kV, 2.8 Torr) and deuterium gas (13.5kV, 3.0 Torr).	126
4.12	The machine, operational and fitting parameters for AECS-PF2.	129
4.13	Information obtained from Lee Model 6-phase code configured for AECS-PF2 at 15kV, 0.41 Torr argon gas.	130
4.14	The machine, operational and fitting parameters for Bora Plasma Focus machine.	132
4.15	Information obtained from Lee Model 5-phase code configured for Bora Plasma Focus machine at 17 kV, 7.6 Torr deuterium gas.	133
4.16	The machine, operational and fitting parameters for HU PF with anode length of 18cm (2.9 Torr) and 22 cm (1.4 Torr) respectively.	135
4.17	Information obtained from Lee Model 6-phase code for HU PF which was configured to work at 16 kV, 2.9 Torr deuterium gas (using 18 cm anode).	136
4.18	Information obtained from Lee Model 6-phase code for HU PF which was configured to work at 16 kV, 1.4 Torr deuterium gas (using 22 cm anode).	137
4.19	The machine, operational and fitting parameters for GN1 Plasma Focus machine with anode radius 1.8 cm and length 12 cm.	141

		Page
4.20	Information obtained from Lee Model 6-phase code configured for GN1 Plasma Focus machine at 30 kV, 0.75 Torr deuterium gas.	141
4.21	The machine, operational and fitting parameters for GN1 Plasma Focus machine with anode radius 1.9 cm and length 8.7 cm.	144
4.22	Information obtained from Lee Model 6-phase code configured for GN1 Plasma Focus machine at 30 kV, 0.75 Torr deuterium gas.	145
4.23	The machine, operational and fitting parameters for GN1 Plasma Focus machine with 8.5 cm anode, 12.6 μ F capacitor.	147
4.24	Information obtained from Lee Model 6-phase code configured for GN1 Plasma Focus machine at 30 kV, 3 Torr deuterium gas (using anode radius 1.9 cm and length 8.5 cm, 12.6 μ F capacitor).	149
4.25	The machine, operational and fitting parameters for FNII Plasma Focus machine.	153
4.26	Information obtained from Lee Model 5-phase code configured for FNII Plasma Focus machine at 36kV, 2.75 Torr deuterium gas.	154
4.27	The machine, operational and fitting parameters for INDIA-ASSAM Plasma Focus machine.	155
4.28	Information obtained from Lee Model 6-phase code configured for INDIA-ASSAM Plasma Focus machine at 19 kV, 0.4 Torr deuterium gas.	156
4.29	The machine, operational and fitting parameters for NX3 Plasma Focus machine operated at different voltages and different pressures in deuterium gas.	158
4.30	Current and mass factor for the fitting of the computed waveform at 12kV, 2.28 Torr deuterium gas.	159

		Page
4.31	Current and mass factors for the fitting of the computed waveform at 12kV, 3.75 Torr deuterium gas and anomalous resistance values.	160
4.32	Current and mass factors for the fitting of the computed waveform at 13kV, 3.0 Torr deuterium gas; and anomalous resistance values.	161
4.33	Current and mass factors for the fitting of the computed waveform at 14kV, 3.75 Torr deuterium gas; and anomalous resistance values.	163
4.34	Computed pinch parameters for NX3 Plasma Focus machine working at different pressures and charge voltages.	164
4.35	The machine, operational and fitting parameters for the BARC Plasma Focus 2 machine. The information was obtained from Dr Rabindra Kumar Rout.	169
4.36	Information obtained from Lee Model 5-phase code configured for the BARC Plasma Focus 2 machine at 24 kV, 3.0 Torr deuterium gas.	170
4.37	The machine, operational and fitting parameters for PF143 Plasma Focus machine working at 1.5 Torr and 9.75 Torr respectively.	172
4.38	Information obtained from Lee Model 6-phase code configured for PF143 Plasma Focus machine at 30kV, 1.5 Torr deuterium gas.	173
4.39	Information obtained from Lee Model 6-phase code configured for PF143 Plasma Focus machine at 30kV, 9.75 Torr deuterium gas.	174
4.40	The machine, operational and fitting parameters for DPF78 Plasma Focus machine.	178
4.41	Information obtained from Lee Model 5-phase code configured for DPF78 Plasma focus machine at 60kV, 7.6 Torr deuterium gas.	179

4.42	The machine, operational and fitting parameters for Tamu Plasma Focus machine.	182
4.43	Information obtained from Lee Model 5-phase code configured for Tamu Plasma Focus machine at 30kV, 12.0 Torr deuterium gas.	183
4.44	The machine, operational and fitting parameters for Posideon Plasma Focus machine.	184
4.45	Information obtained from Lee Model 5-phase code configured for Posideon Plasma Focus machine at 60kV, 3.8 Torr deuterium gas.	185
4.46	Computed and experimental neutron yield as compared to different pressure and voltages for Posideon Plasma Focus machine [16].	186
4.47	The machine, operational and fitting parameters for PF1000 Plasma Focus machine.	188
4.48	Information obtained from Lee Model 5-phase code configured for PF1000 Plasma Focus machine at 27kV, 3.5 Torr deuterium gas.	190
CHAPTER 5		
5.1	The machine, operational and fitting parameters of INDIA-Mohanty's Plasma Focus machine for different anode lengths in nitrogen gas medium.	193
5.2	The parameters of the anomalous resistances for the for INDIA-Mohanty's Plasma Focus machine that uses different anode lengths in nitrogen gas medium.	194
5.3	Computed properties of INDIA-Mohanty's Plasma Focus machine using 5 different anode lengths.	197
5.4	Computed current sheath speed of plasma of INDIA-Mohanty's Plasma Focus machine at 25kV, 0.3 Torr nitrogen gas.	198

		Page
5.5	The machine, operational and fitting parameters for Sofia Plasma Focus machine.	202
5.6	Information obtained from Lee Model 5-phase code configured for Sofia Plasma Focus machine at 16kV, 1.05 Torr nitrogen gas.	203
5.7	The machine, operational and fitting parameters for Zimbabwe Plasma Focus machine.	206
5.8	Information obtained from Lee Model 6-phase code configured for Zimbabwe Plasma Focus machine at 13kV, 1.0 Torr nitrogen gas.	207
5.9	Information obtained from Lee Model 6-phase code configured for Zimbabwe Plasma Focus machine for nitrogen gas at 13 kV compared to the experimental values (air) obtained from Table 2, page 4574 of reference [122].	208
5.10	The machine, operational and fitting parameters for the Nano Focus machine.	209
5.11	Information obtained from Lee Model 5-phase code configured for Nano Focus machine at 6.5kV, 2.25Torr hydrogen gas.	210
5.12	The machine, operational and fitting parameters for Quaid I Azam University Plasma Focus machine.	212
5.13	Information obtained from Lee Model 6-phase code configured for Quaid I Azam University Plasma Focus machine at 20kV, 0.38 Torr hydrogen gas.	213
5.14	The machine, operational and fitting parameters for Egypt Plasma Focus machine.	214
5.15	Information obtained from Lee Model 5-phase code configured for Egypt Plasma Focus machine at 15kV, 0.8 Torr helium gas.	215
5.16	The machine, operational and fitting parameters for PFMA-1 Plasma Focus machine working in helium gas.	216

		Page
5.17	Information obtained from Lee Model 5-phase code configured for the PFMA-1 Plasma Focus machine at 20.5kV, 9.8 Torr helium gas.	217
5.18	The machine, operational and fitting parameters for Rico Plasma Focus machine.	218
5.19	Information obtained from Lee Model 6-phase code configured for Rico Plasma Focus machine at 14.9kV, 0.2 Torr oxygen gas.	219
5.20	The machine, operational and fitting parameters for PF3 Plasma Focus machine.	220
5.21	The machine, operational and fitting parameters for Dena Plasma Focus machine.	223
5.22	The machine, operational and fitting parameters for SPEED2 Plasma Focus machine.	228
5.23	The machine, operational and fitting parameters for UMDPF1 Plasma Focus machine.	230
5.24	Information obtained from Lee Model 5-phase code configured for UMDPF1 Plasma Focus machine at 14 kV, 7.6 Torr deuterium gas.	231
CHAPTER 6		
6.1	Parameters corresponding to optimum computed neutron yield for the machines named below (1/3).	237
6.2	Parameters corresponding to computed optimum neutron yield for the machines named below (2/3).	238
6.3	Parameters corresponding to computed optimum neutron yield for the machines named below (3/3).	239
6.4	Parameters corresponding to computed neon SXR for the machines named below.	243
6.5	Parameters corresponding to computed total argon all-line yield for the machines named below.	247

LIST OF FIGURES

	Page
CHAPTER 1	
1.1 Mather and Filippov type Dense Plasma Focus devices schematic drawing [35, 36].	4
1.2 The physical basis, structure, results and extensive scope of the Lee Model code [57, 58, 63].	8
1.3 Plasma Focus device with current sheet position [83].	10
CHAPTER 2	
2.1 The flow chart showing the fitting procedure for using Lee codes.	18
2.2 The 5-point fitting of current trace to the measured current trace obtained from INTI Plasma Focus (INTI PF) machine (a T2) fired at 2.0 Torr in neon gas.	20
2.3 The 6-point fitting of computed current trace to the measured current trace obtained from INTI PF machine fired at 2.0 Torr in neon gas.	22
2.4 Expanded (zoom in) region of Point 6 to show how the anomalous resistance phase was fitted.	23
2.5 General overview of the NX2 apparatus [6].	25
2.6 NX2 Plasma Focus schematic of electrodes and chamber [6].	25
2.7 INTI Plasma Focus device schematic diagram [84].	27
CHAPTER 3	
3.1 Measured current waveform of PF50 at 29kV, 6.8 Torr deuterium gas compared with Lee Model 5-phase code computed current waveform.	31
3.2 Variation of computed and measured neutron yield in PF50 plasma focus machine with respect to pressure when capacitor is charged to 29kV in deuterium gas.	32

		Page
3.3	Variation of computed and measured neutron yield in PF50 plasma focus machine with respect to pressure when capacitor is charged to 25kV in deuterium gas.	33
3.4	The measured current waveform of INDIA-BARC Plasma Focus 1 machine at 4.2 kV, 1.2 Torr hydrogen gas compared with Lee Model 6-phase code computed current waveform.	35
3.5	The measured current waveform of INDIA-BARC Plasma Focus 1 machine at 4.3 kV, 1.2 Torr deuterium gas compared with Lee Model 6-phase code computed current waveform.	37
3.6	Variation of computed neutron yield with respect to pressure operating at 4.3 kV in deuterium for INDIA-BARC PF1.	38
3.7	The picture of the system used in Alameda Applied Sciences Corporation system which is taken from Figure 1, page 4 of reference [107].	39
3.8	The measured current waveform of AASC Plasma Focus machine at 4 kV, 2.9 Torr deuterium gas compared with Lee Model 6-phase code computed current.	41
3.9	Variation of computed neutron yield with respect to pressure operating at 14 kV in deuterium for AASC Plasma Focus machine.	42
3.10	Picture of Argentina Nano focus machine taken from Figure 5, page 79 of reference [28].	43
3.11	The measured current waveform of Argentina Nano Focus machine at 16 kV, 1.5 Torr deuterium gas compared with Lee Model 5-phase code computed current waveform.	44
3.12	Computed tube voltage versus time for Argentina Nano Focus machine at 16kV, 1.5 Torr deuterium.	45
3.13	Computed inductance variation with time for Argentina Nano Focus machine at 16kV, 1.5 Torr deuterium.	45

		Page
3.14	Variation of computed neutron yield with respect to pressure operating at 16 kV in deuterium for Argentina Nano Focus machine.	46
3.15	Schematic of Composite anode geometry used in FMPF-1	48
3.16	The measured current waveform of FMPF-1 Plasma Focus machine at 12kV, 2.25 Torr deuterium gas compared with Lee Model 5-phase code computed current waveform.	49
3.17	Variation of computed and experimental neutron yield with respect to pressure operating at 12 kV in deuterium for FMPF-1 Plasma Focus machine.	50
3.18	Photograph of India's smallest sealed- type Plasma Focus machine which was obtained from Figure 2, page 026104-2 of reference [108].	51
3.19	The measured current waveform of India's smallest sealed Plasma Focus machine at 10 kV, 6.0 Torr deuterium gas compared with Lee Model 6-phase code computed current waveform.	53
3.20	Variation of computed neutron yield with respect to pressure operating at 10 kV in deuterium for India's smallest sealed Plasma Focus machine.	54
3.21	Neutron yield variation with shot number and with days, taken from Figure 4, page 026104-3 of reference [98].	54
3.22	Measured current waveform of PF400 Plasma Focus machine at 28kV, 6.6 Torr deuterium gas compared with Lee Model 5-phase code computed current waveform.	56
3.23	Variation of computed and experimental neutron yield with respect to pressure operating at 2.8 kV in deuterium for PF400 Plasma Focus machine.	57
3.24	Computed PF400 radial start time and time to peak current versus pressure.	58

		Page
3.25	Measured Pinch time (●) and time to peak current vs filling pressure (▲) taken from Figure 2, page 3270 of reference [26]	58
3.26	Variation of computed and experimental soft X-ray yield with respect to pressure operating at 10 kV in neon for NX1 Plasma Focus machine with anode length of 4.5cm.	61
3.27	The measured current waveform of NX1 Plasma Focus machine at 10kV, 3.0 Torr neon gas, with anode length of 4.5cm compared with Lee Model 6-phase code computed current waveform.	62
3.28	The measured current waveform of NX1 Plasma Focus machine at 14kV, 11.0 Torr neon gas, with anode length of 5.4cm compared with Lee Model 5-phase code computed current.	64
3.29	Variation of computed and experimental soft X-ray yield with respect to pressure operating at 14 kV in neon for NX1 Plasma Focus machine with anode length of 5.4cm.	65
3.30	Variation of computed and experimental focus time with respect to pressure operating at 14 kV in neon for NX1 Plasma Focus machine with anode length of 5.4cm.	65
3.31	Variation of computed and experimental axial speed with respect to pressure operating at 14 kV in neon for NX1 Plasma Focus machine with anode length of 5.4cm.	66
3.32	Measured current waveform of PPRC Plasma Focus machine at 14.2kV, 0.3 Torr argon gas compared with Lee Model 6-phase code computed current waveform.	68
3.33	Measured current waveform of PPRC Plasma Focus machine at 18.5kV, 0.15 Torr argon gas compared with Lee Model 6-phase code computed current waveform.	69

		Page
3.34	Measured current waveform of PPRC Plasma Focus machine at 19kV, 0.7 Torr argon gas compared with Lee Model 6-phase code computed current waveform.	70
3.35	Measured current waveform of PPRC Plasma Focus machine at 18kV, 0.3 Torr argon gas compared with Lee Model 6-phase code computed current waveform.	71
3.36	The measured current waveform of KSU-PF2 Plasma Focus machine at 17kV, 3.0 Torr deuterium gas compared with Lee Model 6-phase code computed current waveform.	74
3.37	Variation of computed neutron yield with respect to pressure operating at 17 kV in deuterium for KSU-PF2 Plasma Focus machine.	75
3.38	The measured current waveform of KSU-PF2 Plasma Focus machine with 125 nH inductance at 1.125 Torr neon gas compared with Lee Model 6-phase code computed current waveform.	76
3.39	Variation of soft X ray yield with respect to pressure operating at 17 kV in deuterium for KSU-PF2 Plasma Focus machine	77
3.40	The measured current waveform of Imperial College Plasma Focus machine at 38kV, 2.62 Torr deuterium gas compared with Lee Model 5-phase code computed current waveform.	79
3.41	Variation of computed and experimental neutron yield with respect to pressure operating at 38 kV in deuterium for Imperial College Plasma Focus machine.	80
3.42	Variation of computed and experimental soft X-ray yield with respect to pressure operating with an anode length of 5cm, 11 kV in neon for NX2 Plasma Focus machine (C1).	83
3.43	Measured current waveform of NX2 at 11kV, 2.6 Torr neon gas and anode length of 5cm compared with Lee Model 5-phase code computed current waveform (C1).	84

		Page
3.44	Measured current waveform of NX2 at 11.5kV, 1.5 Torr neon gas and anode length of 7cm compared with Lee Model 5-phase code computed current waveform (C2).	84
3.45	Variation of computed and experimental soft X-ray yield with respect to pressure operating with an anode length of 7cm, 11.5 kV in neon for NX2 Plasma Focus machine (C2).	85
3.46	Variation of computed and experimental soft X-ray yield with respect to pressure operating with an anode length of 4cm, 11.5 kV in neon for NX2 Plasma Focus machine (C3).	86
3.47	Measured current waveform of NX2 at 11.5kV, 6.0 Torr neon gas compared with Lee Model 5-phase code computed current waveform (C3).	87
3.48	Measured current waveform of NX2-T at 12.5kV, 10.6 Torr deuterium gas compared with Lee Model 5-phase code computed current waveform.	89
3.49	Variation of computed and experimental neutron yield with respect to pressure operating at 12.5 kV in deuterium for NX2-T Plasma Focus machine.	90
3.50	Measured current waveform of Paco Plasma Focus machine at 31kV, 1.35 Torr deuterium gas compared with Lee Model 5-phase code computed current waveform.	92
3.51	The computed time to pinch compared with the experimental results for Paco Plasma focus machine at 31kV.	93
3.52	Variation of computed neutron yield with respect to pressure operating at 31 kV in deuterium for Paco Plasma Focus machine.	94
3.53	Measured current waveform of University of Tehran Plasma Focus machine at 19kV, 0.375 Torr argon gas compared with Lee Model 6-phase code computed current waveform (St1).	97

		Page
3.54	Measured current waveform of University of Tehran Plasma Focus machine at 19kV, 0.375 Torr argon gas compared with Lee Model 6-phase code computed current waveform (St2).	98
3.55	Measured current waveform of University of Tehran Plasma Focus machine at 19kV, 0.375 Torr argon gas compared with Lee Model 6-phase code computed current waveform (St3).	98
3.56	Anomalous resistance of all three shots of University of Tehran Plasma Focus machine at 19kV, 0.375 Torr argon gas and averaged values for the three shots.	99
3.57	The variation of axial phase mass factor (if all other factors are constant) and its effect on axial speed on University of Tehran Plasma Focus machine at 19kV, 0.375 Torr argon gas.	101
3.58	The measured current waveform of Montecucolino Plasma Focus machine at 25kV, 2.0 Torr deuterium gas compared with Lee Model 5-phase code computed current waveform.	103
3.59	Variation of computed neutron yield with respect to pressure operating at 25 kV in deuterium for Montecucolino Plasma Focus machine.	104
3.60	Measured current waveform of DPF 2.2 Plasma Focus machine at 18kV, 11.0 Torr deuterium gas compared with Lee Model 6-phase code computed current waveform.	106
3.61	Variation of computed and experimental neutron yield with respect to pressure operating at 18 kV in deuterium for DPF2.2 Plasma Focus machine.	107
CHAPTER 4		
4.1	The measured current waveform of PF12 at 16kV, 3.5 Torr deuterium gas compared with Lee Model 5-phase code current waveform.	110

		Page
4.2	Information obtained from Lee Model 5-phase code configured for PF12 Plasma Focus Machine at 16kV, 3.5 Torr deuterium gas.	111
4.3	The measured current waveform of Amirkabir Plasma Focus machine at 12 kV, 1.26 Torr argon gas compared compared with Lee Model 6-phase code computed current waveform.	114
4.4	Variation of computed and experimental optimum pressure versus capacitor voltage for Amir Kabir Plasma Focus machine working in argon gas.	115
4.5	Variation of computed and experimental total current at pinch time versus voltage at optimum pressure for Amir Kabir Plasma Focus machine working in argon gas.	115
4.6	Variation of computed total line yield with respect to pressure operating at different voltages in argon for Amir Kabir Plasma Focus machine.	116
4.7	The measured current waveform of Amirkabir Plasma Focus machine at 12 kV, 4.5 Torr neon gas compared compared with Lee Model 6-phase code computed current waveform.	119
4.8	Variation of computed and experimental optimum pressure versus capacitor voltage for Amir Kabir Plasma Focus machine working in neon gas.	120
4.9	Variation of computed and experimental total current at pinch time versus voltage at optimum pressure for Amir Kabir Plasma Focus machine working in neon gas.	120
4.10	Variation of computed soft X ray yield with respect to pressure operating at different voltages in neon for Amir Kabir Plasma Focus machine.	121
4.11	Measured current waveform of UNU ICTP PFF machine at 13.5kV, 1.5 Torr argon gas compared with Lee Model 6-phase code computed current waveform.	123

		Page
4.12	Measured current waveform of UNU ICTP PFF machine at 12kV, 2.0 Torr neon gas compared with Lee Model 6-phase code computed current waveform.	123
4.13	Measured current waveform of UNU ICTP PFF machine at 14kV, 2.8 Torr neon gas.compared with Lee Model 6-phase code computed current waveform	124
4.14	Measured current waveform of UNU ICTP PFF machine at 13.5kV, 3.0 Torr deuterium gas compared with Lee Model 6-phase code computed current waveform.	124
4.15	Variation of computed and experimental soft X-ray yield with respect to pressure operating at 14 kV in neon for UNU/ICTP Plasma Focus machine.	127
4.16	Variation of computed neutron yield with respect to pressure operating at 13.5 kV in neon for UNU/ICTP Plasma Focus machine.	128
4.17	The measured current waveform of AECS-PF2 machine at 15kV, 0.41 Torr argon gas compared with Lee Model 6-phase code computed current waveform.	130
4.18	The measured current waveform of Bora Plasma focus machine at 17kV, 7.6 Torr deuterium gas compared with Lee Model 5-phase code computed waveform.	132
4.19	Variation of computed neutron yield with respect to pressure operating at 17 kV in deuterium for Bora Plasma Focus machine.	133
4.20	The measured current waveform of HU PF at 16 kV, 2.9 Torr deuterium gas compared with Lee Model 6-phase code computed current waveform.	136
4.21	The measured current waveform of HU PF at 16 kV, 1.4 Torr deuterium gas compared with Lee Model 6-phase code computed current waveform.	137

		Page
4.22	Variation of computed neutron yield with pressure for different anode lengths in deuterium for HU PF. The maximum neutron yield is 9.7×10^6 n/shot for 14.5 cm anode with peak $v_a=6.3\text{cm}/\mu\text{s}$ and peak $v_s=20\text{cm}/\mu\text{s}$	138
4.23	Variation of computed and experimental optimum pressure with respect to different anode lengths of HU PF.	139
4.24	The measured current waveform of GN1 Plasma Focus machine at 30kV, 0.75 Torr deuterium gas compared with Lee Model 6-phase code computed current waveform.	142
4.25	Variation of computed and experimental arrival time with respect to pressure operating at 30 kV in deuterium for GN1 Plasma Focus machine.	143
4.26	Variation of computed neutron yield with respect to pressure operating at 30 kV (using anode radius 1.8 cm and length 12 cm) in deuterium for GN1 Plasma Focus machine.	143
4.27	The measured current waveform of GN1 Plasma Focus machine at 30kV, 3.0 Torr deuterium gas compared with Lee Model 6-phase code computed current waveform.	145
4.28	Variation of computed and experimental pinch time with respect to pressure operating at 30 kV (using anode radius 1.9 cm and length 8.7 cm) in deuterium for GN1 Plasma Focus machine.	146
4.29	Variation of computed and experimental neutron yield with respect to pressure operating at 30 kV (using anode radius 1.9 cm and length 8.7 cm) in deuterium for GN1 Plasma Focus machine.	146
4.30	The measured current waveform of GN1 Plasma Focus machine at 30kV, 3.0 Torr deuterium gas compared with Lee Model 6-phase code computed current waveform.	148

		Page
4.31	Computed tube voltage versus time as obtained from Lee Model 6-phase code configured for GN1 Plasma Focus machine at 30 kV, 3 Torr deuterium gas (using anode radius 1.9 cm and length 8.5 cm, 12.6 μ F capacitor).	149
4.32	The maximum pinch voltage on the deuterium filling pressure (estimated in published paper) compared to maximum tube voltage versus pressure from Lee Model 6-phase code.	151
4.33	Variation of computed neutron yield with respect to pressure operating at 30 kV (using anode radius 1.9 cm and length 8.5 cm, 12.6 μ F capacitor) in deuterium for GN1 Plasma Focus machine.	151
4.34	Measured current waveform of FNII Plasma Focus machine at 36kV, 2.75 Torr deuterium compared with Lee Model 5-phase code computed current waveform.	153
4.35	Variation of computed and experimental neutron yield with respect to pressure operating at 36 kV in deuterium for FNII Plasma Focus machine.	154
4.36	The measured current waveform of India Assam Plasma Focus machine working at 19kV deuterium compared with Lee Model 6-phase code computed current waveform.	157
4.37	Variation of computed and experimental neutron yield with respect to pressure operating at 19 kV in deuterium for India Assam Plasma Focus machine.	157
4.38	Measured current waveform of NX3 at 12kV, 2.28 Torr deuterium gas compared with Lee Model 5-phase code computed current waveform ($f_m=0.18$, $f_c=0.7$, $f_{mr}=0.1$ and $f_{cr}=0.7$).	159

		Page
4.39	Measured current waveform of NX3 at 12kV, 3.75 Torr deuterium gas compared with Lee Model 6-phase code computed current waveform ($f_m=0.13$, $f_c=0.7$, $f_{mr}=0.1$ and $f_{cr}=0.7$).	160
4.40	Measured current waveform of NX3 at 13kV, 3.0 Torr deuterium gas compared with Lee Model 6-phase code computed current waveform ($f_m=0.195$, $f_c=0.7$, $f_{mr}=0.1$ and $f_{cr}=0.7$).	162
4.41	Measured current waveform of NX3 at 13kV, 3.0 Torr deuterium gas compared with Lee Model 6-phase code computed current waveform ($f_m=0.172$, $f_c=0.7$, $f_{mr}=0.1$ and $f_{cr}=0.7$).	163
4.42	Variation of computed neutron yield with respect to pressure operating at 12 kV in deuterium for NX3 Plasma Focus machine.	165
4.43	Variation of computed energy input into plasma with respect to pressure operating at 12 kV in deuterium for NX3 Plasma Focus machine.	165
4.44	Variation of computed neutron yield with respect to pressure operating at 14 kV in deuterium for NX3 Plasma Focus machine.	166
4.45	Variation of computed energy input into plasma with respect to pressure operating at 14 kV in deuterium for NX3 Plasma Focus machine.	167
4.46	The measured current waveform of BARC Plasma Focus 2 machine at 24kV, deuterium gas compared with Lee Model 5-phase code computed current for deuterium gas.	169
4.47	Variation of computed and experimental neutron yield with respect to pressure operating at 24 kV in deuterium for INDIA-BARC PF2.	170

		Page
4.48	The measured current waveform of PF143 Plasma Focus machine at 30kV, 1.5 Torr deuterium gas compared with Lee Model 6-phase code computed current waveform.	173
4.49	The measured current waveform of PF143 Plasma Focus machine at 30kV, 9.75 Torr deuterium gas compared with Lee Model 6-phase code computed current waveform.	174
4.50	The compression time of plasma from the peak value to the end of the radial phase as defined in Figure 1, page 250 of reference [126].	175
4.51	Variation of computed and experimental compression time with respect to pressure operating at 30 kV in deuterium for PF143.	175
4.52	Variation of computed and experimental neutron yield with respect to pressure operating at 30 kV in deuterium for PF143.	176
4.53	Measured current waveform of DPF78 at 60kV, 7.6 Torr deuterium gas compared with Lee Model 5-phase code computed current waveform.	178
4.54	DPF78 measured I_{total} (labeled as I_{ges}) and measured I_p waveforms. The third trace I_{is} is the difference of I_{total} and I_p .	179
4.55	Ratio of measured I_p to I_{total} as a function of time [128].	180
4.56	Variation of computed neutron yield with respect to pressure operating at 36 kV in deuterium for DPF78.	180
4.57	Variation of computed neutron yield with respect to pressure operating at 30 kV in deuterium for Tamu PF.	181
4.58	The measured current waveform of Tamu Plasma Focus machine at 30kV, 12.0 Torr deuterium gas compared with Lee Model 5-phase code computed current waveform.	182

		Page
4.59	The measured current waveform of Posideon Plasma Focus machine at 60kV, 3.8 Torr deuterium gas compared with Lee Model 5-phase code computed current.	185
4.60	Variation of computed and experimental neutron yield with respect to pressure operating at 60 kV in deuterium for POSIDEON PF.	187
4.61	Measured current waveform of PF1000 at 27kV, 3.5 Torr deuterium gas compared with Lee Model 5-phase code computed current waveform.	189
4.62	Variation of computed neutron yield with respect to pressure operating at 27 kV in deuterium for PF1000 plasma focus machine.	190
CHAPTER 5		
5.1	The measured current waveforms (anode of 110 mm-figure (a) and anode 115 mm-figure (b)) of INDIA-Mohanty's Plasma Focus machine at 25kV, 0.3 Torr nitrogen gas compared with Lee Model 6-phase code computed current.	195
5.2	The measured current wave forms (anode of 120 mm-figure(c), anode 125 mm-figure (d) and anode 130 mm-figure (e)) of INDIA-Mohanty's Plasma Focus machine at 25kV, 0.3 Torr nitrogen gas compared with Lee Model 6-phase code computed current.	196
5.3	Published average speed compared to computed average speed for different anode lengths of INDIA-Mohanty's Plasma Focus machine at 25kV, 0.3 Torr nitrogen gas.	199
5.4	Ch5 shows the estimated time taken from the start of plasma to the pinch of a 13cm anode and Ch 3 shows the estimated time taken in a 12 cm anode for INDIA-Mohanty's Plasma Focus machine.	200

		Page
5.5	Computed soft X-ray yield versus pressure (a) and experimental soft X-ray yield versus pressure (b) for INDIA-Mohanty's Plasma Focus machine.	201
5.6	The measured current waveform for Sofia Plasma Focus machine at 16kV, 1.05 Torr nitrogen gas compared with Lee Model 5-phase code computation.	203
5.7	Variation of computed soft X ray yield with respect to pressure operating at 16 kV in nitrogen for Sofia Plasma Focus machine.	204
5.8	The measured current waveform for Zimbabwe Plasma Focus machine at 13kV, 1.0 Torr nitrogen gas compared with Lee Model 6-phase code computed current waveform.	207
5.9	Measured current waveform of the Nano Focus machine at 6.5kV, 2.25 Torr hydrogen gas compared with Lee Model 5-phase code computed current waveform.	210
5.10	The measured current waveform of Quaid I Azam University Plasma Focus machine at 20kV, 0.38 Torr hydrogen gas compared with Lee Model 6-phase code computed current.	213
5.11	The measured current waveform of Egypt Plasma Focus machine at 15kV, 0.8 Torr helium gas compared with Lee Model 5-phase code computed current waveform.	215
5.12	The measured current waveform of PFMA-1 Plasma Focus machine at 20.5kV, 9.8 Torr helium gas compared with Lee Model 5-phase code computed current waveform.	217
5.13	The measured current waveform of Rico Plasma Focus machine at 14.9kV, 0.2 Torr oxygen gas compared with Lee Model 6-phase code computed current waveform.	219
5.14	Measured current waveform of Filippov PF3 Plasma Focus at 9kV, 1.5 Torr neon gas compared with Lee Model 5-phase code computed current waveform.	221

		Page
5.15	Radial trajectory of Filippov PF3 according to the Lee Model 5-phase code; taken from same numerical shot as Figure 5.14.	222
5.16	Measured current waveform of Filippov Dena Plasma Focus at 16kV, 0.5 Torr argon gas compared with Lee Model 5-phase code computed current waveform.	224
5.17	Siahpoush's Modified Lee [ML] code used to fit Dena Plasma Focus machine [41]; with our additional small adjustments: time shifted 0.3 microseconds and the amplitude reduced by 1 %. These small adjustments significantly improve the fit.	226
5.18	The measured current waveform at 180kV, 1.875Torr deuterium gas compared with Lee Model 5-phase code computed current waveform.	228
5.19	The measured current waveform compared with Lee Model 5-phase code computed.	230
5.20	Variation of computed neutron yield with respect to pressure when capacitor in UMDPF1 Plasma Focus machine is charged to 14kV in deuterium gas.	231
CHAPTER 6		
6.1	3 kJ UNU ICTP PF.	233
6.2	1 MJ PF1000 Plasma Focus.	233
6.3	Computed neutron yield versus input energy in the Plasma Focus machine.	236
6.4	Neutron yield versus input energy Neutron yield versus input energy (All data-computed and measured)..	240
6.5	Computed neutron yield versus peak current.	240
6.6	Computed neutron yield versus pinch current.	241
6.7	Computed peak current versus energy input into plasma.	241
6.8	Computed pinch current versus energy input into plasma.	242

		Page
6.9	Computed neutron yield versus pinch duration.	242
6.10	Computed neon soft X-ray yield versus pinch current.	244
6.11	Computed neon soft X-ray yield versus peak current.	245
6.12	Computed neon soft X ray versus energy input into plasma.	245
6.13	Computed energy input into plasma versus pinch duration	246
6.14	Computed line yield versus peak current.	247
6.15	Computed line yield versus pinch current.	248
6.16	Computed line yield versus energy input into plasma.	248